Design strategy for controlled natural aging in Al–Mg–Si alloys

M. Werinos [a], H. Antrekowitsch [a], T. Ebner [b], R. Prillhofer [b], W.A. Curtin [c], P.J. Uggowitzer [d], S. Pogatscher [a*]

[a] Institute of Nonferrous Metallurgy, Montanuniversitaet Leoben, Franz-Josef-Strasse 18, 8700 Leoben, Austria

[b] AMAG Rolling GmbH, Postfach 32, 5282 Ranshofen, Austria

[c] Institute of Mechanical Engineering, EPFL, 1015 Lausanne, Switzerland

[d] Laboratory of Metal Physics and Technology, Department of Materials, ETH Zurich, Vladimir-Prelog-Weg 4, 8093 Zurich, Switzerland

This study presents a design strategy for Al–Mg–Si alloys to control natural aging. Recently, trace addition of Sn was shown to suppress natural aging for up to two weeks, which was explained by the strong trapping of vacancies to Sn atoms. Here we explore the effect of solution treatment temperature, the combination of trace elements such as Sn and In, and the composition of main hardening elements Mg, Si and Cu on natural aging. The results are discussed based on the dissolvable amount of trace elements and their effect on diffusion retardation, and solute clustering mechanisms in Al–Mg–Si alloys. Thermodynamic calculations using the CALPHAD approach show that maximum retardation of natural aging is achievable at the highest trace element solubility, which exists at significantly different solution treatment temperatures for Sn or In. The effects of Mg, Si and Cu content on natural aging kinetics are interpreted via their influence on the Sn solubility and clustering mechanisms. It is proposed that Sn additions reduce the concentration of excess vacancies, which is most important for early Si clustering, and that the effect of Cu is comparable to the effect of Sn, but less pronounced. Based on the investigated parameter space, a design concept is proposed and an Al–Mg–Si alloy showing suppression of natural aging for > 6 months and significant artificial aging potential is demonstrated.

Keywords: aluminum alloys, natural aging, phase transformation kinetics, vacancies, trace elements

1. Introduction

Age hardenable Al–Mg–Si alloys (6xxx-series) are widely used in the transport, automotive, shipbuilding, and aviation industry [1–3]. Aluminum allows lightweight construction for improved fuel efficiency and reduced CO_2-emissions. 6xxx-series alloys are especially attractive as they combine good formability with medium to high strength after age hardening, good corrosion resistance, and weldability. In the automotive industry, for example, they are used as outer skin alloys, for non-decorative inner parts, and structural or crash components with individual property criteria [1–5]. Yet, the ever-growing demand to increase formability and strength for more complex parts of lower weight drives the alloy development considerably [4–7].

The delivery of semi-finished products mostly occurs after quenching to enable forming operations at low strength prior to the final heat treatment to gain high strength [4,8–10]. During natural aging (n.a.), which starts directly after quenching from solution heat treatment, the material hardness increases due to solute clustering of Mg- and Si-atoms [11–15]. This generates two problems for the transportation industry: first, dynamic hardening during n.a. reduces formability [4]; second, clustering results in a negative effect of n.a. on subsequent artificial aging (a.a.) [12,13,16–18]. The transportation industry, however, requires several months of stable formability combined with good a.a. performance so as to obtain reproducibility of designs that have increasing complexity [4,10]. Hence, pre-aging treatments have been developed to improve a.a. and to achieve a relatively “stable” material state [8,10,19–22]. Pre-aging treatments, however, result in undesired hardness increase [10].

This study presents a novel design strategy for 6xxx-alloys to achieve maximal suppression of n.a. hardening after quenching while still achieving a potential for significant a.a. The study builds on recent research showing that trace tin (Sn) addition to the alloy AA6061 can suppress n.a. for 2 weeks and simultaneously improve the a.a. potential [23–25].

Here, detailed investigation of the effects of solution treatment temperature and Mg, Si and Cu content in alloys, with and without trace element additions, leads to a designed Al–Mg–Si alloy showing n.a. stability for more than 6 months.

2. Methods

Table 1 shows the alloys studied here. Alloys 1-13 were produced at the laboratory scale starting from AA6061 base alloys. After re-melting, pure Mg, Si, Cu, Sn or Sn+In were added to the base alloys to obtain the compositions listed in Table 1. Ar gas purging was applied to reduce the hydrogen content before the alloys were cast to slabs. After cutting and homogenization, hot rolling was conducted. To check the chemical composition of the final sheets, optical emission spectrometry and, for In, inductively coupled plasma mass spectroscopy, were used. Alloys 14 and 15 with and without Sn addition were industrially produced and supplied by AMAG rolling GmbH in the form of wrought plates. Note that all chemical compositions in Table 1 are near to commercial AA6061 alloys.

Table 1: Composition of alloys (Al in balance)

Alloy	**Symbol**	Sn	Sn	In	Mg	Si	Cu	Fe	Mn	Cr	Zn	Ti
	MgSiCu	[at.ppm]	[wt.%]	[wt.%]	[wt.%]	[wt.%]	[wt.%]	[wt.%]	[wt.%]	[wt.%]	[wt.%]	[wt.%]
1	↓↓↓	430	0.188		0.82	0.63	0.232	0.59	0.111	0.147	0.059	0.079
2	↓↓↓	96	0.042		0.78	0.61	0.210	0.493	0.119	0.154	0.045	0.040
3	↓↓↓	70	0.030		0.79	0.58	0.213	0.482	0.11	0.147	0.057	0.088
4	↓↓↓	6	0.0026		0.81	0.62	0.220	0.485	0.111	0.146	0.059	0.081
5	~~~	94	0.041		0.87	0.72	0.300	0.510	0.118	0.148	0.045	0.041
6	↑~~	94	0.041		0.96	0.71	0.288	0.456	0.116	0.147	0.044	0.043
7	↓~~	96	0.042		0.77	0.73	0.298	0.462	0.117	0.148	0.045	0.042
8	~↑~	91	0.040		0.85	0.83	0.287	0.449	0.116	0.147	0.045	0.043
9	~↓~	94	0.041		0.86	0.61	0.245	0.456	0.116	0.148	0.045	0.042
10	~~↑	91	0.040		0.84	0.70	0.379	0.443	0.115	0.150	0.043	0.043
11	~~↓	89	0.039		0.86	0.74	0.203	0.476	0.116	0.151	0.045	0.044
12	↓↓↓	98	0.043	0.039	0.78	0.62	0.211	0.5	0.118	0.152	0.045	0.039
13	~~~	91	0.040	0.04	0.84	0.71	0.245	0.447	0.115	0.150	0.043	0.044
14	↓⬇↑	96	0.042		0.78	0.434	0.357	0.455	0.109	0.136	0.047	0.056
15	↓⬇↑	5	0.002		0.76	0.411	0.355	0.452	0.109	0.138	0.045	0.053

Solution heat treatment of hardness test samples was performed in a circulating air furnace (Nabertherm N60/85 SHA) at temperatures between 510-570 °C for 1.2×10^3 s. Subsequent quenching was carried out in water at room temperature and, for n.a., samples were kept in a Peltier-cooled incubator IPP (Memmert) at 25 °C. Artificial aging was undertaken in an oil bath.

Brinell hardness measurements (HBW 2.5/62.5) were carried out using an EMCO-Test M4 unit. A maximum standard deviation of 2.0 HBW was achieved.

Thermodynamic calculations of the alloys were performed using FactSage™ 6.4 software [11] together with the FACT FTlite light alloy database (2014). For the equilibrium calculations the alloy compositions according to Table 1 were entered and all possible phases selected from the databases. Data of phases and their stabilities, compositions and element solubility were calculated between 320 °C and 600 °C.

3. Results

3.1. Influence of solution treatment temperature

Figures 1 and 2 show the effect of solution treatment temperature on n.a. kinetics of alloys 1-3 containing 430, 96 and 70 at. ppm Sn, respectively, and alloy 4 (Table 1). Alloy 4 represents the "Sn-free" reference alloy with low Mg, Si and Cu content (↓: low, symbol: ↓↓↓) and commercial amounts of impurity elements (compare ref. [23]). A solution heat treatment at 570 °C is compared to 550 °C, 530 °C and 510 °C. After annealing at 570 °C, the alloys containing 430 and 96 at. ppm Sn preserve the as-quenched hardness for ~14 days (Fig. 1a). The alloy with 70 at. ppm Sn starts hardening after more than 4 days (Fig. 1b). At lower solution treatment temperatures hardening starts earlier, followed by a steep logarithmic increase in hardening. Between 530 °C and 570 °C, all alloys reach comparable hardness maxima, which is in contrast to a lower peak hardness after annealing at 510 °C.

The "Sn-free" reference alloy 4 starts hardening within minutes and exhibits similar kinetics after all solution treatment temperatures (Fig. 2). Between 530 °C and 570 °C, hardness values are similar. After annealing at 510 °C, in contrast, the alloy shows ~5-8 HBW lower hardness until 360 days. The final hardness maxima, however, are comparable to the Sn-added alloys 1-3 after same heat treatments.

3.2 Addition of In as a second trace element

To elucidate the effect of combined Sn and In addition on n.a. kinetics (Fig. 3), alloys 12 (symbol: ↓↓↓) and 13 (symbol: ~~~) with low or average Mg, Si and Cu content contain ~0.04 wt.% In (~100 at. ppm, Table 1) in addition to ~0.04 wt.% Sn. Figure 3 shows the n.a. curves after annealing at 530 °C and 570 °C. The In-added low-alloyed alloy starts hardening after ~14 days nearly independent of solution treatment temperature. The In-added average alloy shows slightly retarded hardening kinetics after 530 °C compared to annealing at 570 °C.

3.3 Influence of Mg, Si and Cu content

To evaluate the influence of Mg, Si and Cu on n.a. kinetics for alloys with Sn addition, Fig. 4-6 compare the average alloy 5 (symbol: ~~~; for Mg Si Cu), with alloys containing ~0.1 wt.% higher (↑: high) or lower (↓: low) concentrations of the corresponding element (Table 1). After annealing at 570 °C (Fig. 4a-6a) the average alloy starts hardening after ~1 day; after 530 °C (Fig. 4b-6b) n.a. starts earlier. Alloys 8 (symbol: ~↑~) and 9 (symbol: ~↓~) with high or low Si content demonstrate a significant influence of Si on hardening kinetics (Fig. 4). After both solution treatment temperatures, a higher Si content (0.83 wt.%) results in earlier hardening than the average alloy. With lower Si content (0.61 wt.%) hardening is retarded, starting after ~7 days after annealing at 570 °C (Fig. 4a). For Mg-variation (Fig. 5,

alloys 6 and 7), a weaker effect on n.a. kinetics is found, although the trend is similar to Si: a lower Mg content produces slightly retarded n.a. hardening and vice versa. Cu variations (Fig. 6) show a general tendency to marginally retard hardening with increasing Cu content.

Further, for the alloy with high Si content, significantly higher initial hardness values are measured after annealing at 570 °C. The same applies for high Mg content, but less pronounced as compared to Si. For Cu variations, no significant shift of the initial hardness is seen.

3.4 Thermodynamic calculations

The thermodynamic calculations in Fig. 7 show the temperature-dependent Sn solubility in the fcc Al matrix between 320 °C and 600 °C for alloys 1, 3 and 14 (Table 1). The low alloyed alloys with 430 and 70 at. ppm Sn show the maximum solubility of Sn at 570 °C (Fig. 7). At lower temperature the solubility decreases. Similar values were calculated for alloy 2, but for the sake of clarity not shown in Fig. 7. The same trend applies for alloy 14, but at 570 °C it exhibits a higher Sn solubility.

For combined Sn and In addition, the thermodynamic calculations in Fig. 8 show two contrary effects of the Sn and In solubility for alloys 12 and 13, with low and average Mg, Si and Cu content, respectively. The higher the Sn solubility, the lower the solubility of In and vice versa, because with decreasing temperature, the In solubility increases.

To evaluate the influence of Si, Mg and Cu on Sn solubility, Figs. 9a-c compare the thermodynamic calculation of the average alloy 5 to alloys 6-11 with varied element contents. According to the calculations, Si addition (in blue) significantly reduces the Sn solubility at temperatures above ~550 °C and below 530 °C (Fig. 9a). An opposite effect is found for lower Si content (in pink). Similar to Si, Fig. 9b indicates a lower Sn solubility for higher Mg

concentrations. For Cu variations, the thermodynamic calculations between 0.20 and 0.38 wt.% Cu do not suggest any influence on the Sn solubility (Fig. 9c).

4. Discussion

The results showed that n.a. kinetics of the Sn-added Al–Mg–Si alloys is significantly influenced by the Sn content, the solution treatment temperature applied, the Mg, Si and Cu content and additional trace elements.

4.1 Solution treatment temperature

The n.a. results of alloys 1-3 with 430, 96 and 70 at. ppm Sn in Fig. 1 showed after solution heat treatments between 570 °C and 510 °C earlier hardening with decreasing temperature. In contrast, the n.a. kinetics of the "Sn-free" reference alloy 4 showed no dependence on solution treatment temperature (Fig. 2). The lower hardness level of the alloy after annealing at 510 °C is supposed to result from the reduced Mg and Si solubility at this temperature in fcc Al, because of the solvus temperature of Mg_2Si being >510 °C (not depicted). The same applies for the lower peak hardness of alloys 1-3 at 510 °C. The other results can be interpreted with the Sn solubility calculations in Fig. 7.

For the solution heat treatments applied, it is assumed that the total amount of Sn dissolved at the solution treatment temperature is quenched-in, resulting in a concentration of Sn in fcc Al c_{Sn} at room temperature. This implies that the maximum quenchable c_{Sn} is limited by the Sn solubility at a given solution treatment temperature. According to the calculations in Fig. 7, at lower temperature the Sn solubility decreases, which reduces c_{Sn} at room temperature. To quantify the retardation of n.a. hardening at temperature T due to Sn additions, we recently proposed a retardation factor R [23] which shows a linear dependency on c_{Sn},

$$R = 1 + 12c_{Sn}(e^{\Delta E_{SV}/kT}) \quad (1)$$

Where ΔE_{SV} is the solute-vacancy binding energy and k the Boltzmann's constant. Thus the link between the influence of solution treatment temperature on retardation of n.a. hardening (Fig. 1) and the calculated temperature-dependency of the Sn solubility (Fig. 7) can be easily established. A lower quenched-in c_{Sn} at room temperature with decreasing solution treatment temperature explains why alloys 1, 2 and 3 start hardening earlier (Fig. 1). Thus the calculated Sn solubility values are expected to give accurate trends, if not absolute values.

The Sn solubility at 570 °C for alloys 1-3 was calculated to be ~55 at. ppm. From this calculation one would expect no difference in hardening retardation since the Sn content of all alloys is above this value. However, the 70 at. ppm Sn alloy starts hardening earlier than the 96 and 430 at. ppm Sn alloys (compare Fig. 1a and 1b). Alloy 2 with 96 at. ppm and alloy 3 with 430 at. ppm Sn, on the other hand, start hardening at nearly the same time. From this observation we assume that the real Sn solubility of alloys 1-3 is higher than the calculated 55 at. ppm, namely >70 ppm but ≦100 at. ppm. Indeed, the Sn solubility in an AA6061 alloy containing a Mg, Si and Cu content comparable to alloys 1-3 was experimentally found to be ~100 at. ppm after annealing at 570 °C [23]. Consequently, it is assumed that the 96 and 430 at. ppm Sn alloys generate comparable quenched-in c_{Sn}, which explains the similar hardening kinetics (Fig. 1a). Based on these results, the Sn content in alloys 5-14 was adjusted at ~100 at. ppm.

4.2 Additional trace elements

Equation 1 predicts that the retardation of n.a. hardening also depends on the strong Sn-vacancy binding energy ΔE_{SV} (~0.24-0.3 eV [23,26,27]). The Sn addition is envisioned to result in trapping of excess vacancies, which reduces the amount of untrapped vacancies in the Al matrix that control diffusional processes. Consequently, any diffusional processes, like

clustering, are slowed down [23]. Yet, this favorable trapping of excess vacancies is limited by the Sn solubility at the solution treatment temperature (section 4.1). Therefore a second element with strong solute-vacancy binding energy, if soluble in fcc Al, is expected to increase the effect of Sn on n.a. kinetics.

To evaluate the effect of combined trace element addition, a diffusion retardation factor R for two different types of trace elements is required. The thermodynamic model assumes two types of dilute solutes dissolved in fcc Al after quenching, with the solute concentrations much higher than the total quenched-in vacancy concentration at the effective quench temperature T_Q [28], $c_S^{(1)}$ and $c_S^{(2)} \gg c_V^{tot}(T_Q)$. During quenching, some excess vacancies are trapped in solute-vacancy pairs at the beginning of n.a. at temperature T (solute-divacancy arrangements, or similar, types of configuration are assumed to be negligible). Only the residual untrapped vacancy concentration $c_V(T)$ is present to control any vacancy-mediated diffusional processes. Thus, n.a. hardening is retarded by a factor $R = c_V^{tot}(T_Q)/c_V(T)$. Following the lines of the derivation in ref. [23] and with the solute-vacancy binding energies ΔE_{SV} of each solute type denoted with a superscript, the retardation factor is

$$R = \frac{c_V(T_Q)}{c_V(T)} = \frac{1+12c_S^{(1)}(e^{\Delta E_{SV}^{(1)}/kT})+12c_S^{(2)}(e^{\Delta E_{SV}^{(2)}/kT})}{1+12c_S^{(1)}(e^{\Delta E_{SV}^{(1)}/kT_Q})+12c_S^{(2)}(e^{\Delta E_{SV}^{(2)}/kT_Q})} \quad (2)$$

For sufficient high T_Q, the denominator approaches 1 and can be neglected. Thus, the retardation factor for combined trace element addition is approximately

$$R = 1 + 12c_S^{(1)}(e^{\Delta E_{SV}^{(1)}/kT}) + 12c_S^{(2)}(e^{\Delta E_{SV}^{(2)}/kT}) \quad (3)$$

According to Eq. 3, In fulfills both preconditions to be effective in the retardation of n.a. hardening: (i) it shows a strong solute-vacancy binding energy of ~0.20 eV [26] and (ii) thermodynamic calculations indicate a reasonable solubility in fcc Al (see Fig. 8).

Compared to the solely Sn-added alloys 2 and 5 of comparable composition, the In-added alloys 12 and 13 with low or average Mg, Si and Cu content show significantly

retarded n.a. hardening after annealing at 530 °C, while n.a. kinetics after 570 °C are only reduced slightly (compare Fig. 3 to alloy 2 in Fig. 1a and alloy 5 in Fig. 4-6). This can be explained by the trend toward increasing In solubility at lower solution treatment temperatures (Fig. 8). It is concluded that the effect of trace elements on retardation of n.a. hardening can be expanded to a broad solution treatment temperature range by a combination of Sn and In additions. However, this effect is limited by the mutual influences on element solubility as shown in Fig. 8.

4.3 Influence of Mg, Si and Cu content and mechanisms

The influence of Mg, Si and Cu content on n.a. kinetics in Fig. 4-6 can be interpreted with the Sn solubility curves in Fig. 9 and considering clustering mechanisms in Al–Mg–Si alloys.

According to Fig. 9a, an increase in Si content reduces the Sn solubility at the solution treatment temperatures investigated and thus reduces c_{Sn}. According to Eq. 1, the reduction of c_{Sn} at 570 °C by a factor of ~1.8 should increase n.a. kinetics by the same factor. The ratio of hardening onset times in Fig. 4a is, however, ~20, decreasing from ~7 days (alloy 9) to ~8 h (alloy 8). Although the computed values of c_{Sn} might be not totally accurate, it is not expected that the error of the thermodynamic calculations is sufficient to account for the observed differences. Thus the lower c_{Sn} only partly explains the observed earlier n.a. hardening for higher Si content (Fig. 4).

We compare our findings with the latest research on n.a. clustering in Sn-free Al–Mg–Si alloys. At the beginning of n.a., clustering is dominated by solute-vacancy complexes (stage I). In the following clustering stage II, the fraction of vacancy-free clusters continuously increases until these dominate [15]. Both types of clusters are interpreted as predominantly involving Si and result in an increase of electrical resistivity or hardening at an

initial rate in stage I and a more rapid increase in stage II [13,14,29,30]. Both linear logarithmic stages are present in the hardening curves in Fig. 1-6. With exception of a recent study by Kim et al. [31], most studies on n.a. kinetics of Sn-free Al–Mg–Si alloys including the effect of Si show, unfortunately, only results for ≥ 60 min n.a. [16,32], so that the first stages are not revealed. The only effect observed is a higher n.a. hardness for alloys with increased Si content. Note that the same effect is observable here for Si variations in Fig. 4. In ref. [31] an earlier onset of n.a. hardening is seen the higher the Si content. All studies, including those focusing on the influence of Si content on a.a. kinetics [16,31–33], interpret the higher n.a. hardness or better a.a. performance of high Si-alloyed Al–Mg–Si alloys (e.g. 6016) as being primarily influenced by the early clustering processes [16] and rapidly forming Si(-rich) clusters [31–33], respectively. A higher Si content can be consequently expected to increase early stage clustering kinetics during n.a. [13,14,29,31,34]. The higher initial hardness for high Si content after annealing at 570 °C (Fig. 4a), in contrast, may be attributed to pre-existing Si clusters formed during quenching. Indirect evidence of faster hardening kinetics at higher Si content is given in ref. [34,35] where a pure Al-Mg-Si alloy is compared to an alloy with Fe and Mn addition. The slower hardening kinetics of the Fe- and Mn-containing alloy is attributed to the formation of intermetallic phases containing Si. This lowers the quenchable Si-concentration in the matrix and thus the rate of clustering [34]. Summing up, these studies support the hypothesis that Si-related clustering controls the beginning of n.a. and its kinetics [13,14,29–31,36]. This implies that, due to the formation of Si-vacancy complexes, early Si clustering is controlled by the availability of quenched-in excess vacancies (compare ref. [29,30]) because during n.a., vacancies detach from unstable solute-vacancy complexes or vacancy-containing clusters to transport further solute atoms to emerging vacancy-free clusters [29,30,37]. With Sn additions, the formation kinetics of vacancy free-clusters is supposed to be slowed down due to the favorable trapping of

vacancies in stable Sn-vacancy pairs [23], resulting in a reduction of untrapped vacancies available for Si clustering. Thus two trends may produce the accelerated n.a. kinetics at higher Si content in stages I and II (Fig. 4): first, the lower quenched-in c_{Sn} (Fig. 9a) corresponds to fewer trapped vacancies and thus more untrapped vacancies; second, in alloys with higher Si content the vacancy diffusion distances to nearby Si atoms are reduced for untrapped and detached vacancies (compare ref. [38]). A more detailed analysis of the mechanisms involved is the subject of on-going research.

Only in the later clustering stages diffusion of Mg atoms into the emerging clusters does occur (stage III), causing intermediate hardening rate perceived by a transition range before the slowest hardening rate seen at the end of n.a. (stage IV) [13–15,29]. Thus, Mg is believed not to take part in the early clustering processes in stages I and II. Figure 9b shows that Mg addition reduces the calculated Sn solubility by a factor of 1.5 (at 570 °C) to ~2.6 (at 530 °C), which is, at 570 °C, comparable to the difference in retardation of n.a. hardening (Fig. 5). At lower Mg content, the higher quenched-in c_{Sn} favors the trapping of vacancies by Sn and reduces the number of untrapped vacancies. This is presumed to reduce Si clustering in stages I and II and the diffusion velocity of Mg atoms by a comparable factor. Consequently, in contrast to the strong direct effect of Si on early clustering, it is believed that Mg shows only a secondary effect by influencing the Sn solubility. The higher initial hardness for high Mg content after annealing at 570 °C (Fig. 5a) is attributed to solid solution strengthening. The reduced n.a. kinetics of the alloy with high Mg content after annealing at 530 °C may result from a combination of effects: Thermodynamic calculations of the Sn-added alloys show for increased Mg and same Si content a constant Si solubility at 570 °C, whereas at 530 °C the Si solubility already decreases the higher the Mg content, assumingly due to Mg_2Si-Phase formation. Hence, the lower quenched-in Si concentration may reduce

n.a. kinetics while the simultaneously reduced quenched-in c_{Sn} increases n.a. kinetics. For the average alloy with fastest n.a. kinetics one or both effects may contribute weaker.

An increase in Cu content does not influence Sn solubility, but shows a trend toward retardation of n.a. hardening (compare Fig. 5 and 9c). Cu addition to Al–Mg–Si alloys is known to lower the first clustering peak in DSC-measurements that is related to Si clustering in stages I-II and also to reduce early stage n.a. kinetics [34,39–41]. Cu also shows an attractive solute-vacancy binding energy [26,42]. Assuming that Cu stays dissolved in the fcc Al matrix, it may bind vacancies and lower the number of Si-vacancy complexes, which slows down clustering kinetics. This interpretation by ref. [34] is compatible with our interpretation of the effect of Sn on clustering processes in Al–Mg–Si alloys. A higher Cu content may thus add to the effect of Sn in Fig. 5 in some way. But in contrast to Sn, we assume that Cu only weakly immobilizes vacancies, which would explain the weaker effect of Cu on n.a. kinetics.

4.4 Design strategy for maximum retardation of natural aging

Based on the knowledge established through the studies reported above, we propose the following design strategy to obtain Al–Mg–Si alloys with considerably reduced n.a. kinetics:

(i) Identification of the solution treatment temperature with maximum solubility of Sn;

(ii) Detailed adjustment of the Mg, Si and Cu contents according to their individual effects on the solubility of Sn and on early Si clustering;

(iii) Alloying of additional trace elements of high solute-vacancy binding energy.

Step (i) is applicable to any Al–Mg–Si alloy. With thermodynamic calculations of Sn-added alloys, the solution treatment temperature with the highest Sn solubility is computable. For the alloy investigated in this study, this is ~560-570 °C (Fig. 7).

Step (ii) requires understanding of the influence of composition on n.a. kinetics. Compared to the average alloy 5 (Tab. 1), the investigations on alloys within the standards of AA6061 revealed retarded n.a. hardening for low Si- and high Cu-content, and a small effect of Mg on kinetics (Fig. 3-5). However, Cu addition should be treated with care, to still meet the product requirements on corrosion resistivity [43–45].

Step (iii) expands steps (i) and (ii) with a second trace element of high solute-vacancy binding energy and reasonable solubility in the Al–Mg–Si alloy. A significant retardation of n.a. hardening at low solution treatment temperatures (~530 °C) was found with In addition to Sn-added AA6061 (Fig. 6). For industrial application of In, however, the high metal price needs to be considered.

4.5 Designed alloy

In light of the above, we have developed a Sn-added Al–Mg–Si alloy that contains low Mg, very low Si and high Cu content, while remaining within the standards of alloy AA6061 (alloy 14 in Tab. 1, symbol: ↓⬇↑). For reference, we have also prepared a similar alloy, alloy 15, containing essentially no Sn additions. Derived from the strategy steps this approach focuses on identifying the maximum suppression of n.a. hardening with trace Sn addition.

The calculations presented in Fig. 7 confirm that the developed alloy shows the highest calculated Sn solubility in fcc Al of all alloys investigated in this study. Figure 10a compares n.a. hardening curves of the designed alloy 14 with the “Sn-free” alloy 15 of comparable composition. The designed alloy shows improved n.a. stability at both solution treatment temperatures, i.e. after annealing at 530 °C hardening starts after 14 days. After a solution heat treatment at 570 °C, the as-quenched alloy 14 is stable for more than 180 days. Thereafter, it takes ~405 days of n.a. until alloy 14 reaches a peak hardness that is similar to that of the “Sn-free” alloy 15. As further shown in Fig. 10a, the “Sn-free” alloy 15 shows

comparable hardness values and n.a. kinetics for both solution treatment temperatures investigated. But compared to the "Sn-free" alloy 4 with low Mg, Si and Cu content (Fig. 2), alloy 15 reveals significantly slower hardening kinetics, i.e. it starts hardening only after ~3 h and takes more than 90 days to reach maximum hardness. Consequently, Sn-free Al–Mg–Si alloys within the range of commercial compositions can achieve retarded n.a. hardening for low Si and high Cu content.

For applications of Al–Mg–Si alloys, the a.a. performance for optimum strength in service is also required. Figure 10b shows the a.a. performance of the designed alloy 14 after annealing at 570 °C followed by 3 months of n.a.; results for the "Sn-free" alloy 15 are also shown. During a.a. at 185 °C, the designed alloy 14 starts hardening immediately and reaches a maximum hardness of ~103 HBW. After 1800 s of a.a. the "Sn-free" variant shows similar hardness. The inset to Fig. 10b compares the a.a. results after 1800 s to higher a.a. temperatures, i.e. 195 °C, 205 °C, 215 °C, 225 °C and 235 °C. Here, the designed alloy shows the greatest increase in hardness of up to ~97 HBW, which can be explained by unconventional fast a.a. kinetics of Sn-added Al–Mg–Si alloys found at high a.a. temperatures (ref. [24]).

4. Conclusions

The objective of this study was to develop a design strategy to reduce natural aging (n.a.) kinetics of Al–Mg–Si alloys while still achieving a significant artificial aging (a.a.) potential. Through an extensive study across a range of composition space, we have found that

- The addition of trace elements with high solute-vacancy binding energy and reasonable solubility in the Al matrix retards diffusional processes during n.a.

- For maximum retardation of n.a. hardening with trace Sn addition, the application of a high solution treatment temperature is necessary to obtain the maximum quenchable Sn solubility.
- The influences of Mg, Si and Cu content are explained via their effect on Sn solubility and individual effect on clustering. Si increases n.a. clustering kinetics and lowers the quenchable Sn solubility. Cu retards n.a. hardening, but does not influence the Sn solubility and is therefore believed to show a similar, but weaker effect as Sn. Mg lowers the quenchable Sn solubility only.
- Application of a new design strategy has led to the development of a new Sn-added Al–Mg–Si alloy that shows n.a. stability of more than 6 months and a significant a.a. potential.

Overall, the new design strategy and underlying aging mechanisms have the potential to trigger the development of new industrial Al–Mg–Si alloys in general, and especially in the field of transportation industries that have a demand for highly formable materials.

Acknowledgements

The authors thank the Austrian Research Promotion Agency (FFG) and AMAG Rolling for their financial support of this work. WAC thanks the European Research Council for support through an Advanced Grant, “Predictive Computational Metallurgy”, ERC Grant agreement No. 339081 - PreCoMet.

References

[1] Polmear IJ. Light alloys: From traditional alloys to nanocrystals. 4th ed. Oxford, Burlington, MA: Elsevier/Butterworth-Heinemann; 2006.

[2] Ostermann F. Anwendungstechnologie Aluminium. 3rd ed. Berlin, Heidelberg: Springer Berlin Heidelberg; 2014.

[3] Kammer C. Aluminium-Taschenbuch. 16th ed. Düsseldorf: Aluminium-Verl; 2002.

[4] Prillhofer R, Rank G, Berneder J, Antrekowitsch H, Uggowitzer PJ, Pogatscher S. Materials 2014;7:5047–68.

[5] Hirsch J. Transactions of Nonferrous Metals Society of China (English Edition) 2014;24:1995–2002.

[6] Hirsch J. Materials Transactions 2011;52:818–24.

[7] Hirsch J. Materials Forum 2004;28:15–23.

[8] Abouarkoub A, Thompson GE, Zhou X, Hashimoto T, Scamans G. Metallurgical and Materials Transactions A 2015:1–14.

[9] Berneder L, Prillhofer R, Enser J, Grohmann T. TMS Light Metals 2014:177–82.

[10] Birol Y. Materials Science and Engineering A 2005;391:175–80.

[11] Panseri C, Federighi T. Journal of the Institute of Metals 1966;94:99–105.

[12] Kovaćs I, Lendvai J, Nagy E. Acta Metallurgica 1972;20:975–83.

[13] Banhart J, Chang C, Liang Z, Wanderka N, Lay M, Hill A. Advanced Engineering Materials 2010;12:559–71.

[14] Banhart J, Lay M, Chang C, Hill A. Physical Review B 2011;83:14101.

[15] Liu M, Čížek J, Chang C, Banhart J. Acta Materialia 2015;91:355–64.

[16] Brenner, P., Kostron, H. Zeitschrift für Metallkunde 1939;4:89–97.

[17] Ried A, Schwellinger P, Bichsel H. Aluminium 1977;53:595–9.

[18] Pogatscher S, Antrekowitsch H, Leitner H, Ebner T, Uggowitzer P. Acta Materialia 2011;59:3352–63.

[19] Yan Y, Liang ZQ, Banhart J. Materials Science Forum 2014;794-796:903–8.

[20] Miao W, Laughlin D. Journal of Materials Science Letters 2000;19:201–3.

[21] Shen C. Journal of Materials Science and Technology 2011;27:205–12.

[22] Cao L, Rometsch PA, Zhong H, Muddle BC. Materials Science Forum 2010;654-656:918–21.

[23] Pogatscher S, Antrekowitsch H, Werinos M, Moszner F, Gerstl S, Francis MF, Curtin WA et al. Physical Review Letters 2014;112:225701–5.

[24] Werinos M, Antrekowitsch H, Kozeschnik E, Ebner T, Moszner F, Löffler JF, Uggowitzer PJ et al. Scripta Materialia 2016;112:148–51.

[25] Werinos M, Antrekowitsch H, Fragner W, Ebner T, Uggowitzer PJ, Pogatscher S. Influence of Alloy Production History on Natural Aging of AA6061 Modified with Sn, in: GDMB (Ed.). Proceedings of European Metallurgical Conference (EMC) 2015. Clausthal-Zellerfeld: GDMB Verlag GmbH; 2015. p. 303–310.

[26] Wolverton C. Acta Materialia 2007;55:5867–72.

[27] Simonovic D, Sluiter M. Physical Review B - Condensed Matter and Materials Physics 2009;79.

[28] Fischer F, Svoboda J, Appel F, Kozeschnik E. Acta Materialia 2011;59:3463–72.

[29] Chang C, Liang Z, Schmidt E, Banhart J. International Journal of Materials Research 2012;103:955–61.

[30] Chang C, Banhart J. Metallurgical and Materials Transactions A: Physical Metallurgy and Materials Science 2011;42:1960–4.

[31] Kim S, Kim J, Tezuka H, Kobayashi E, Sato T. Materials Transactions 2013;54:297–303.

[32] Hirth SM, Marshall GJ, Court SA, Lloyd DJ. Materials Science and Engineering A 2001;319-321:452–6.

[33] Gupta A, Lloyd D, Court S. Materials Science and Engineering A 2001;316:11–7.

[34] Liang Z. Clustering and Precipitation in Al-Mg-Si Alloys. Phd thesis. Berlin; 2012.

[35] Liang Z, Chang C., Wanderka N., Banhart J., Hirsch J. The Effect of Fe, Mn and Trace Elements on Precipitation in Al-Mg-Si Alloy, in: Proceedings of the 12th International Conference on Aluminium Alloys. p. 492–497.

[36] Zandbergen M, Xu Q, Cerezo A, Smith G. Acta Materialia 2015.

[37] Zurob H, Seyedrezai H. Scripta Materialia 2009;61:141–4.

[38] Torsaeter M, Hasting H, Lefebvre W, Marioara C, Walmsley J, Andersen S, Holmestad R. Journal of Applied Physics 2010;108:073527-1 - 073527-9.

[39] Liang Z, Chang C, Banhart J, Hirsch J. The effect of Cu and Cr on clustering and precipitation in Al–Mg–Si alloys., in: ICAA13: 13th International Conference on Aluminum Alloys: John Wiley & Sons, Inc; 2012. p. 1125–1130.

[40] Zandbergen MW, Cerezo A, Smith G. Acta Materialia 2015.

[41] Kim J, Kobayashi E, Sato T. Materials Transactions 2015;56:1771–80.

[42] Mantina M, Wang Y, Chen L, Liu Z, Wolverton C. Acta Materialia 2009;57:4102–8.

[43] Svenningsen G, Larsen MH, Walmsley J, Nordlien JH, Nisancioglu K. Corrosion Science 2006;48:1528–43.

[44] Wang Zb, Li H, Miao F, Sun W, Fang B, Song R, Zheng Z. Materials Science and Engineering A 2014;590:267–73.

[45] Svenningsen G, Larsen M, Nordlien J, Nisancioglu K. Corrosion Science 2006;48:3969–87.

Figure captions

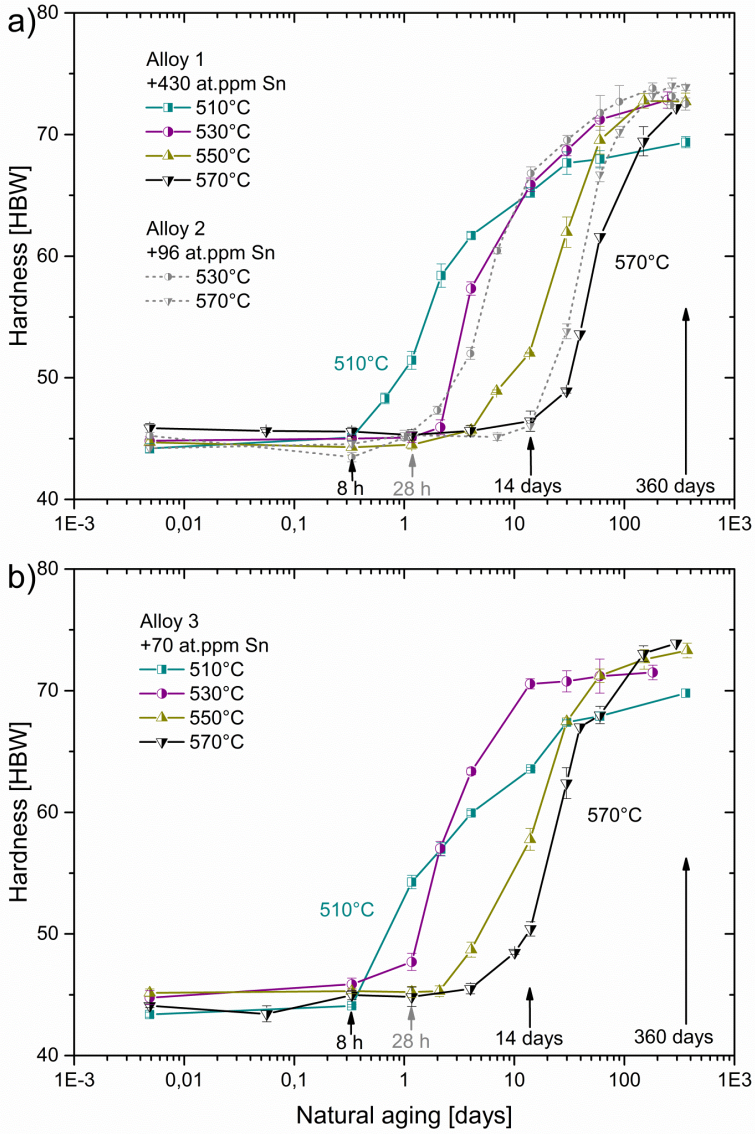

Fig. 1: Influence of solution treatment temperature (570-510 °C) on natural aging kinetics of Sn-added Al–Mg–Si alloys containing a) 430, 96 or b) 70 at. ppm Sn. For all alloys hardening starts earlier at lower solution treatment temperatures.

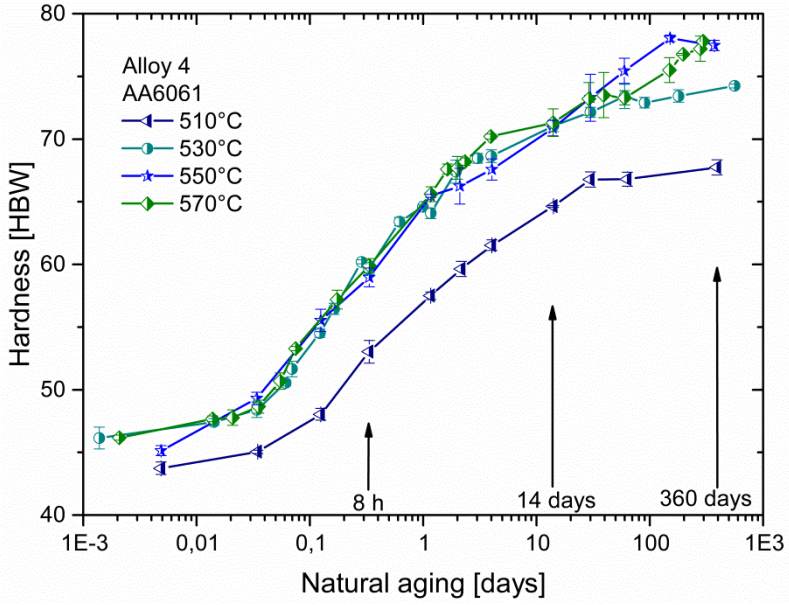

Fig. 2: Influence of solution treatment temperature (570-510 °C) on natural aging kinetics of a commercial, “Sn-free” Al–Mg–Si alloy. The alloy shows similar hardening kinetics for the solutions treatment temperatures investigated.

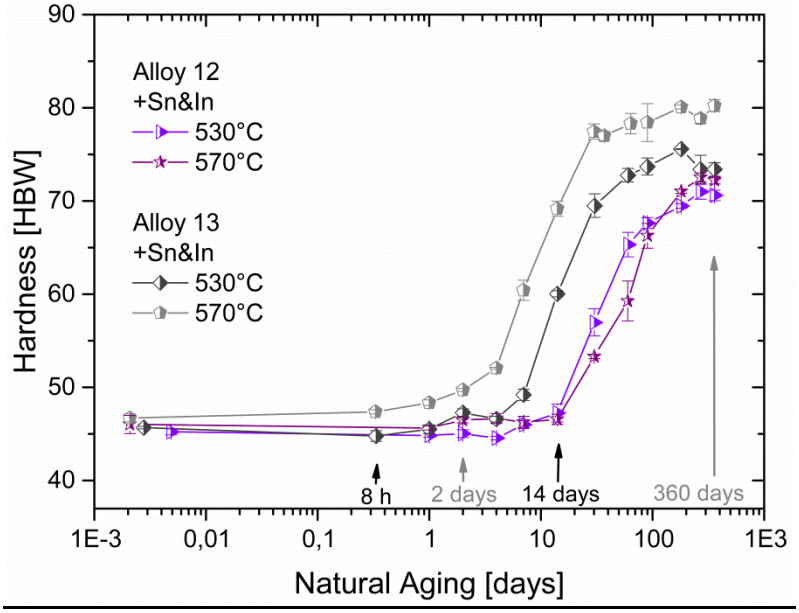

Fig. 3. Natural aging (n.a.) kinetics of two different Sn- and In-added Al–Mg–Si alloys (Tab. 1), annealed at 530 °C and 570 °C. The alloys only show small differences in their hardening kinetics for the solutions treatment temperatures investigated.

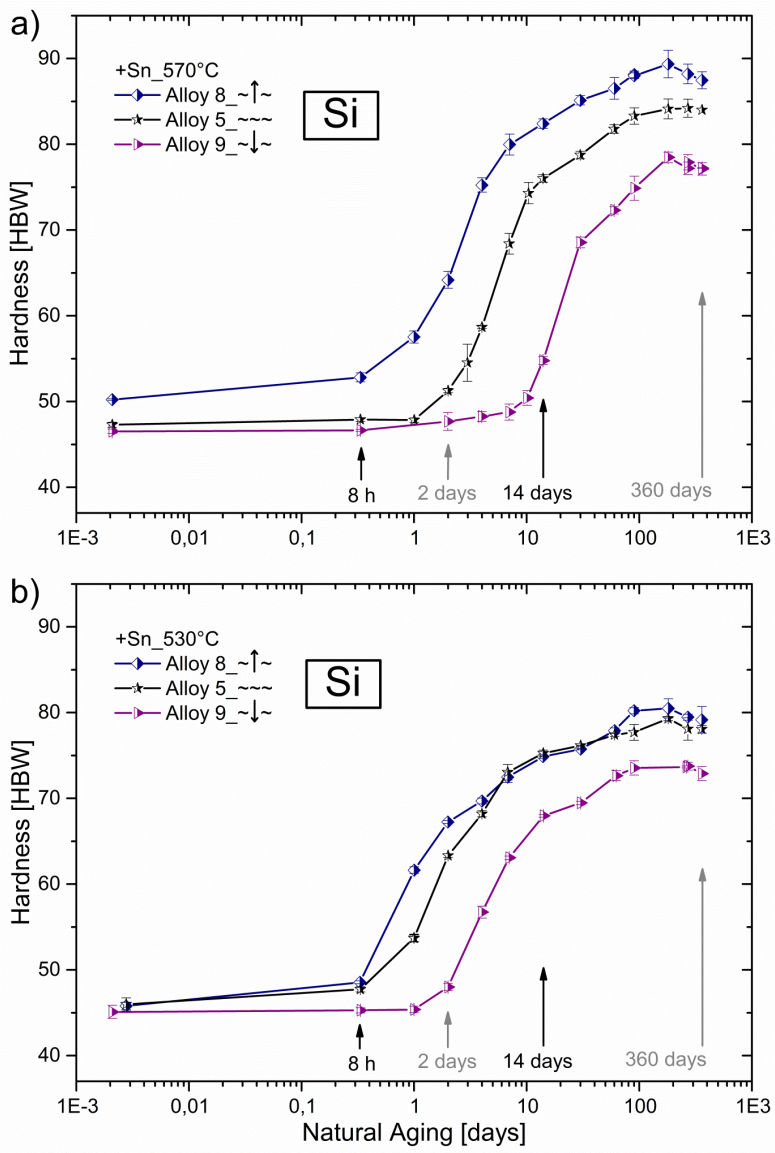

Fig. 4. Influence of Si content on natural aging kinetics of Sn-added Al–Mg–Si alloys annealed at a) 570 °C or b) 530 °C. An alloy with average Mg, Si and Cu content (symbol: ~~~) is compared to alloys with high (↑) or low (↓) Si content (Tab. 1). With lower Si content hardening starts delayed.

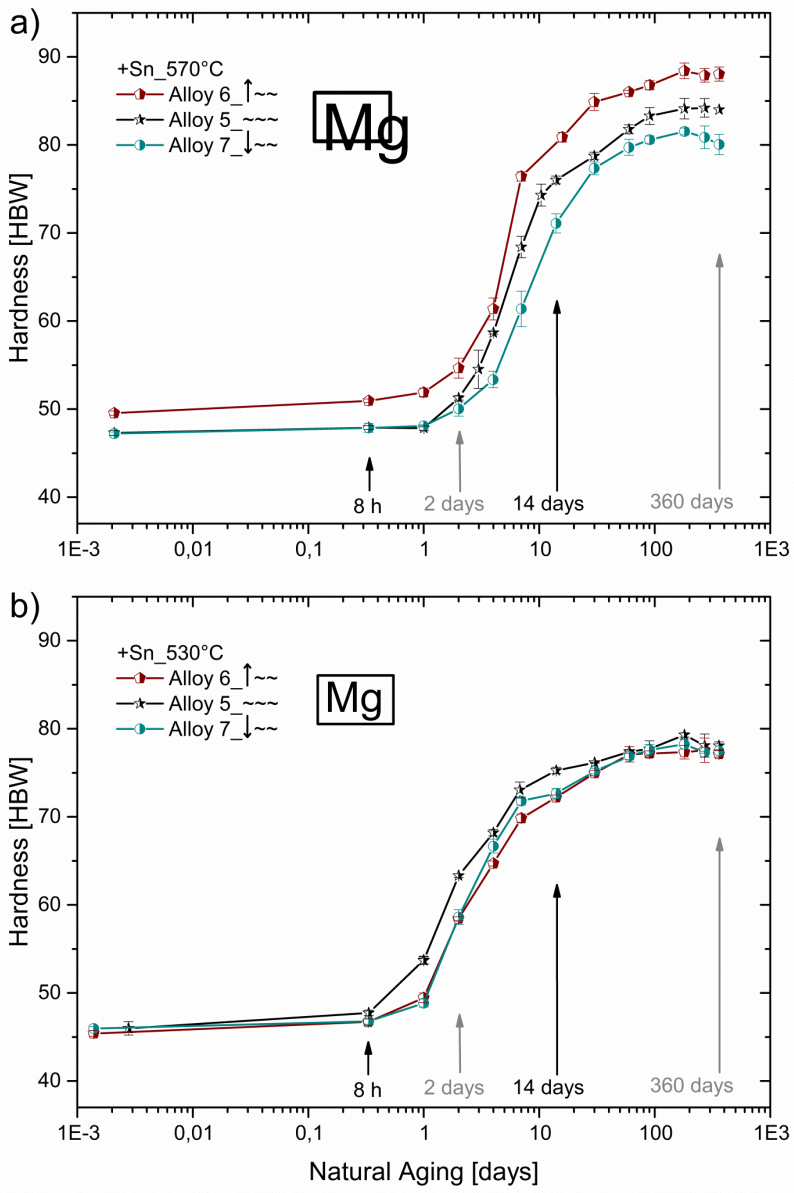

Fig. 5. Influence of Mg content on natural aging kinetics of Sn-added Al–Mg–Si alloys annealed at a) 570 °C or b) 530 °C. An alloy with average Mg, Si and Cu content (symbol: ~~~) is compared to alloys with high (↑) or low (↓) Mg content (Tab. 1). The effect of Mg is not pronounced at 530 °C, but hardening starts delayed for a lower Mg content at 570 °C.

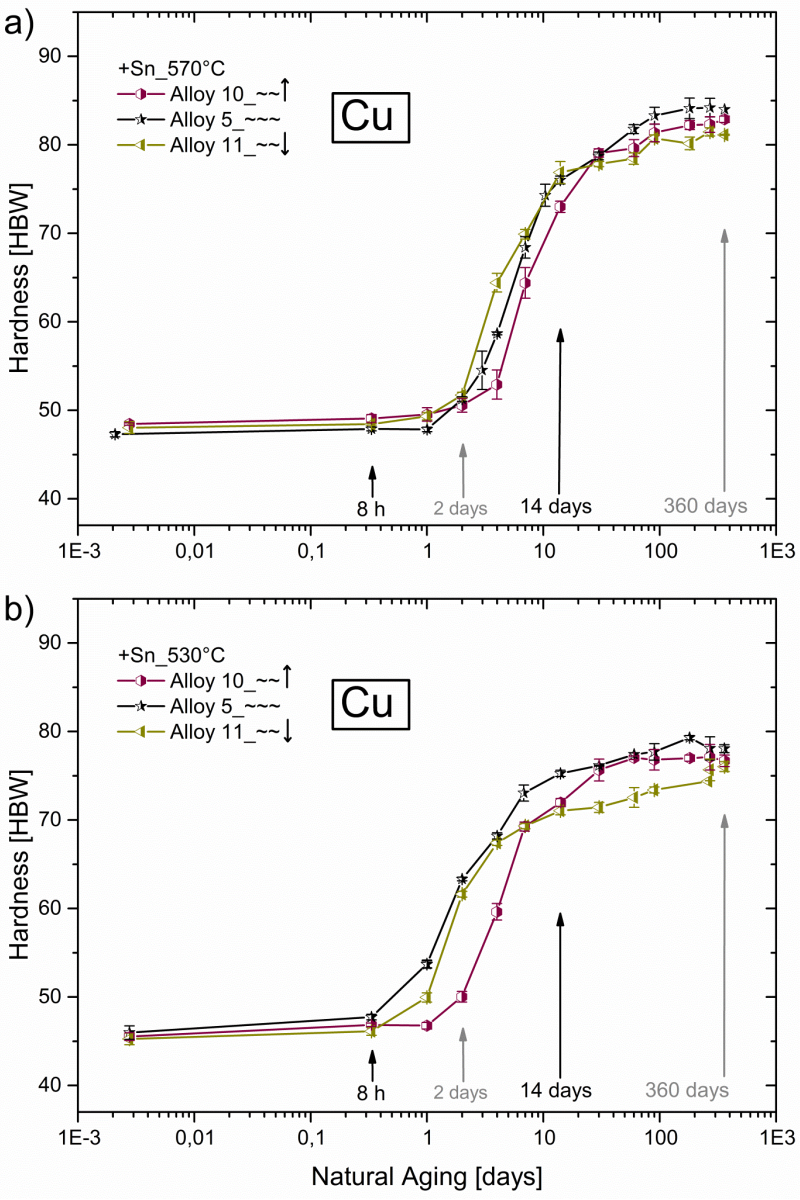

Fig. 6. Influence of Cu content on natural aging kinetics of Sn-added Al–Mg–Si alloys annealed at a) 570 °C or b) 530 °C. An alloy with average Mg, Si and Cu content (symbol: ~~~) is compared to alloys with high (↑) or low (↓) Cu content (Tab. 1). The results show a general tendency to marginally retarded hardening with increasing Cu content.

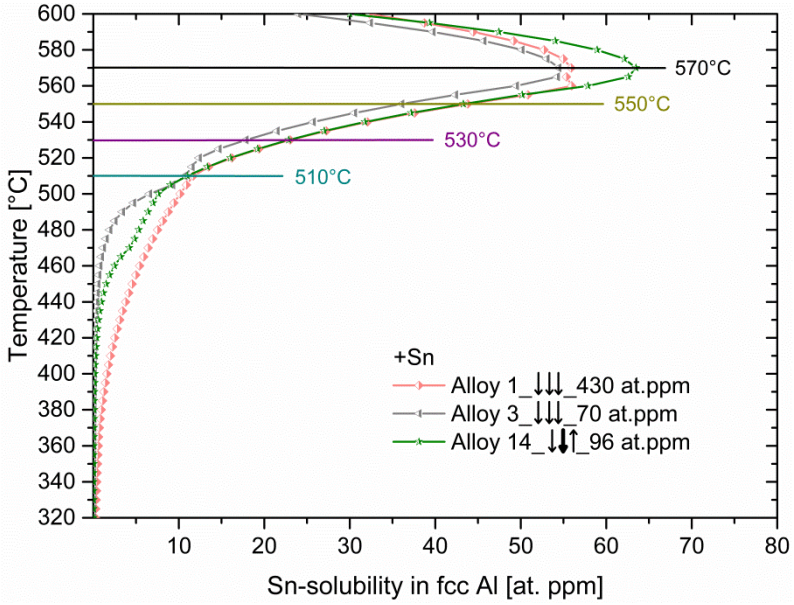

Fig. 7. Calculated temperature dependency of the Sn solubility in fcc Al in Al–Mg–Si alloys containing low Mg, Si and Cu content (symbol: ↓↓↓) or low Mg, very low Si and high Cu content (symbol: ↓⬇↑).

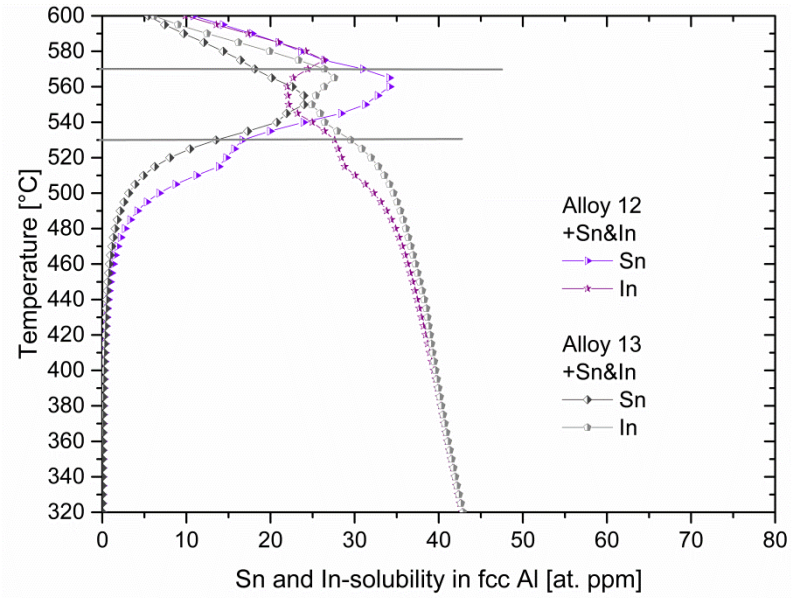

Fig. 8. Calculated temperature dependency of the Sn and In solubility in fcc Al in two different Sn- and In-added Al–Mg–Si alloys (Tab. 1).

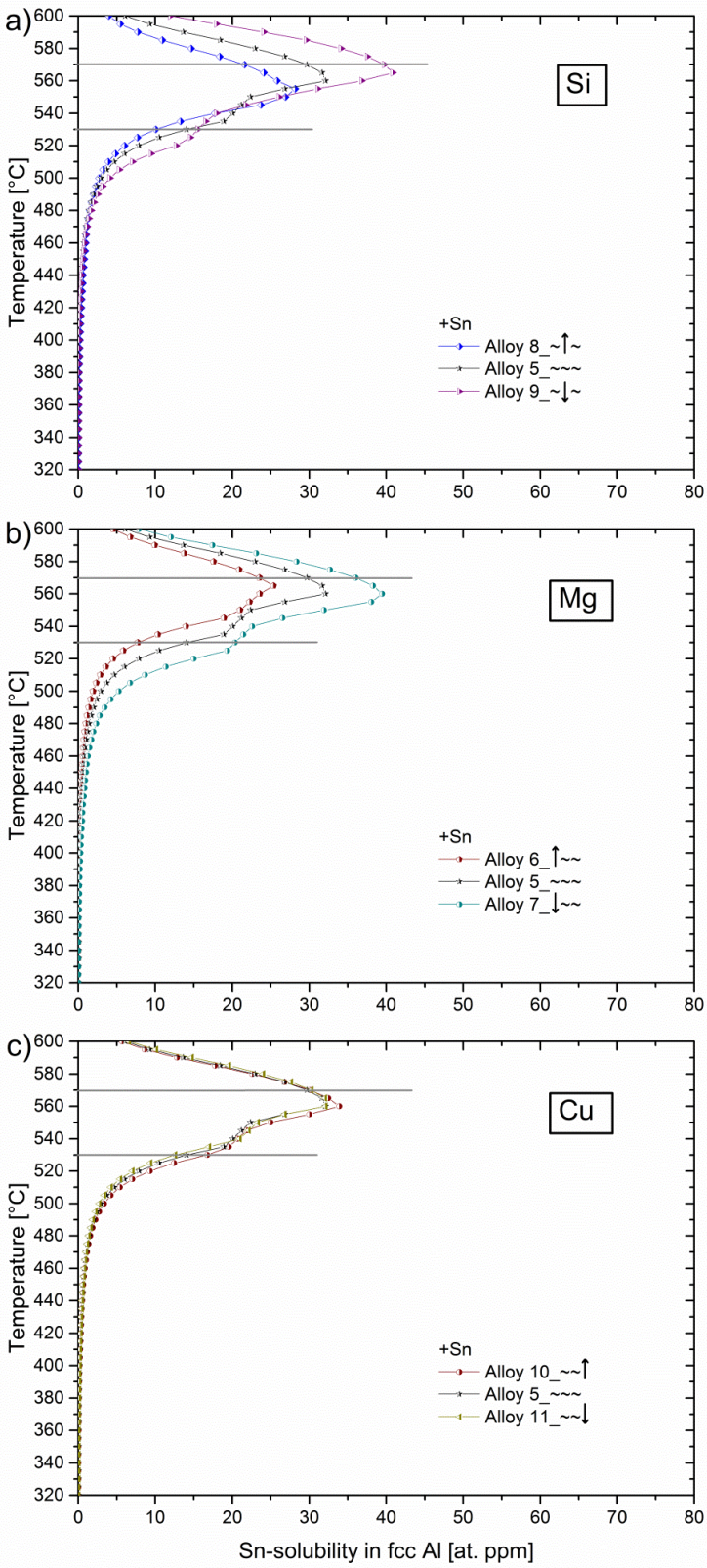

Fig. 9. Influence of the a) Si, b) Mg or c) Cu content on the calculated Sn solubility in fcc Al in Al–Mg–Si alloys. For the nomenclature see Tab. 1 and Fig. 4-6.

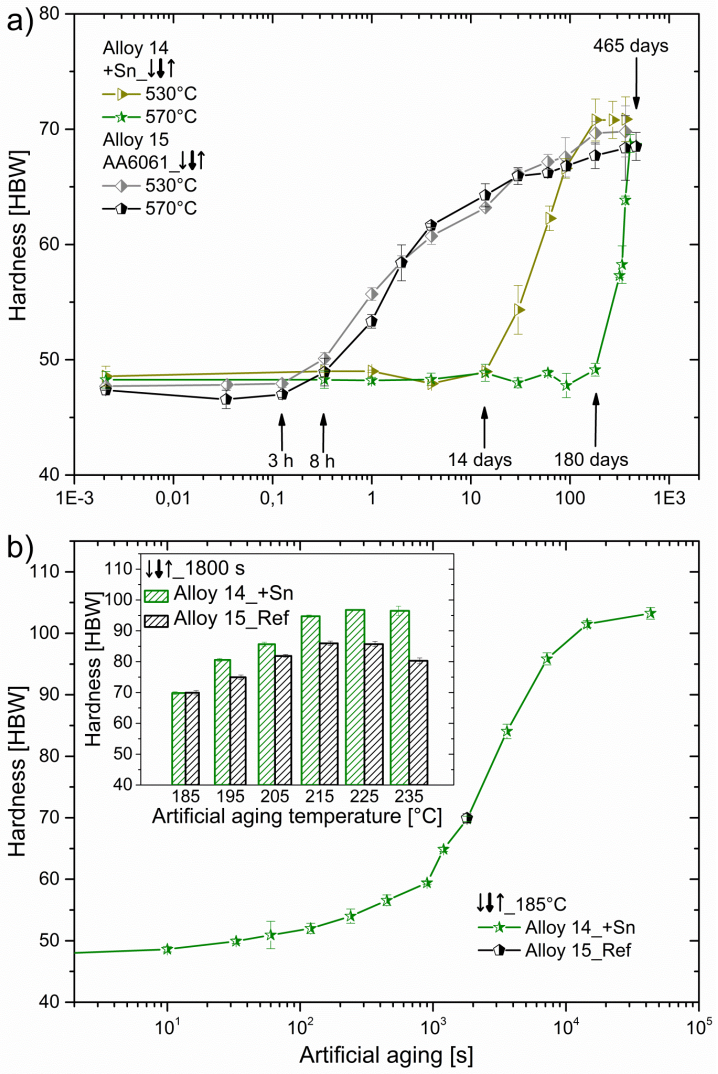

Fig. 10. Aging potential of the designed, Sn-added Al–Mg–Si alloy containing low Mg, very low Si and high Cu content (symbol: ↓⇓↑); results for the "Sn-free" reference alloy are also shown. a) Natural aging (n.a.) kinetics after annealing at 530 °C and 570 °C where after annealing at 570 °C, the designed alloy is stable for >180 days. b) Artificial aging (a.a.) after annealing at 570 °C followed by 3 months of n.a. where the designed alloy shows a significant a.a. potential.

Graphical Abstract